# Magnetically controlled anisotropic light emission of DNA-functionalized supraparticles

Talha Erdem*, Mykolas Zupkauskas, Thomas O'Neill, Alessio Cassiagli, Peicheng Xu, Yemliha Altintas, Evren Mutlugun, and Erika Eiser*

In this article, we show the DNA-functionalization of supraparticles, form their network, and manipulate the optical features of these networks by applying a magnetic field. We start with preparing the supraparticles (SPs) of semiconducting InP/ZnSeS/ZnS quantum dots (QDs), plasmonic silver nanoparticles, and superparamagnetic iron oxide nanoparticles. These SPs are prepared by employing azide-functionalized amphiphilic diblock or triblock copolymers as well as by using their combinations. Subsequently, we attached single-stranded DNAs to these SPs by employing copper-free click chemistry. Next, we hybridized DNA-coated QD SPs with the iron oxide SPs and formed a network. By applying a magnetic field, we restructured this network such that the iron oxide SPs are aligned. This led to an anisotropic emission from the QD SPs with a polarization ratio of 1.9. This study presents a proof-of-concept scheme to control the optical features of a self-assembled supraparticle system using an external interaction. We believe that our work will further contribute to the utilization of smart self-assembly techniques in optics and photonics.

## Impact statement

The self-assembly of the nanoparticles, which lies at the heart of this article, enables achieving unconventional physical responses that cannot be obtained by the individual nanomaterials. Therefore, controlling the self-assembly process can lead to unprecedented control over the mechanical, optical, or electronic features of such novel architectures made of various types of nanoparticles. This smart self-assembly process will undoubtedly enable the realization of novel applications and open new avenues in materials science and engineering. In this article, we employ the self-assembly in two different aspects. First, we self-assembled magnetic, plasmonic, and semiconducting nanoparticles to obtain their supraparticles with the help of various amphiphilic polymers. Next, single-stranded DNA molecules were attached to them for the first time to achieve a precise control over their physical forming a "network of supraparticles of nanoparticles." As a proof-of concept demonstration, we hybridized DNA-functionalized magnetic supraparticles made of iron oxide nanoparticles and DNA-functionalized light-emitting supraparticles containing InP/ZnSe/ZnS quantum dots. We explored the potential of tailoring the emission characteristics of the emitted light by utilizing an external magnetic field. We observed that under an external magnetic field the hybrid network reshapes; as a result, the polarization of the emitted light can be changed such that polarization anisotropy reaches ~1.9. We believe that our work presented here can initiate advanced-level active polarization control in displays and other light-emitting devices in the future. Considering that LCD-based displays require polarized light to function, the results of this work may serve for realizing efficient polarizer-free displays that rely on the manipulation of the structure under the magnetic field.

## Introduction

Colloidal nanoparticles (NPs) promise novel optical, electronic, and magnetic features mostly attributed to their small sizes and large surface-to-volume ratios. Owing to these attractive features, these particles have found applications in various fields, including electronics,[1] photonics,[2–5] mechanics,[6,7] and biology.[8,9] The past few decades have also witnessed their utilization in new fabrication technologies such as nanoimprint lithography,[10] printing,[11,12] and smart self-assembly[13–16] offering cost-effective solutions to fabricate complex and small-sized structures.

Among these, in this work, we are interested in the latter approach, which relies on the controlled, programmed self-assembly of NPs to form desired structures. Although peptide-[17,18] and protein-based[19,20] approaches may be utilized for this purpose, the DNA-based smart self-assembly is one step ahead

Talha Erdem, Departments of Electrical-Electronics Engineering, and Materials Science and Nanotechnology Engineering, Abdullah Gül University, Kayseri, Turkey; Department of Physics, Cavendish Laboratory, University of Cambridge, Cambridge, UK; erdem.talha@agu.edu.tr
Mykolas Zupkauskas, Department of Physics, Cavendish Laboratory, University of Cambridge, Cambridge, UK
Thomas O'Neill, Department of Physics, Cavendish Laboratory, University of Cambridge, Cambridge, UK
Alessio Cassiagli, Department of Physics, Cavendish Laboratory, University of Cambridge, Cambridge, UK
Peicheng Xu, Department of Physics, Cavendish Laboratory, University of Cambridge, Cambridge, UK
Yemliha Altintas, Departments of Electrical-Electronics Engineering, and Materials Science and Nanotechnology Engineering, Abdullah Gül University, Kayseri, Turkey;
Evren Mutlugun, Departments of Electrical-Electronics Engineering, and Materials Science and Nanotechnology Engineering, Abdullah Gül University, Kayseri, Turkey;
Erika Eiser, Department of Physics, Cavendish Laboratory, University of Cambridge, Cambridge, UK; PoreLab, Department of Physics, Norwegian University of Science and Technology, Trondheim, Norway; ee247@cam.ac.uk
*Corresponding author

doi:10.1557/s43577-022-00352-z

of the others owing to the flexibility and programming capability that it proposes.[21–23]

Following the first reports on the self-assembled lattices of DNA-functionalized gold NPs,[24,25] photonically active structures have arisen[26] while the type of NPs of interest has also quickly extended to semiconductor nanocrystal quantum dots (QDs), superparamagnetic NPs, other noble metals, graphene particles, and polymeric colloids.[23,27–30] Our team has recently added the emulsions stabilized by amphiphilic polymers to the family of the DNA-functionalized colloids.[31]

A missing item on this list is the supraparticles (SPs) that are made of many individual NPs within a spherical volume.[32] These SPs, in principle, allow for obtaining functional nanoparticle hybrids in larger dimensions such that the optical and chemical features can be tailored. The size of these particles may range from a few tens of nanometers to hundreds of nanometers depending on the preparation conditions.[33] These SPs have found applications in optically pumped lasers,[34] tunable white light emitters,[35] photothermal therapy and surface-enhanced Raman scattering[36] in addition to magnetic resonance imaging[37] and targeted drug delivery.[38]

In this article, we aim to demonstrate the DNA-functionalization of the SPs, the formation of a network of these SPs, and the manipulation of its optical features by an external effect. With this motivation, we prepared the SPs of InP/ZnSeS/ZnS core/shell/shell nanocrystal QDs, silver NPs, and iron oxide NPs. To stabilize the SPs, we used diblock and triblock copolymers that we functionalized with azide groups. We subsequently employed the copper-free click chemistry to DNA-functionalize our SPs and studied the DNA conjugation efficiency on different surfactant types. Next, we self-assembled these SPs using Watson–Crick interaction and demonstrated the control of emission polarization of semiconductor-magnetic supraparticle hybrids using magnets.

## Experimental methods

### Nanoparticle synthesis

Iron oxide NPs in toluene are purchased from Sigma-Aldrich. InP/ZnSeS/ZnS QDs are synthesized according to the literature[39] with modifications in the synthesis recipe,[40] and hydrophobic silver NPs are synthesized according to literature by Farrell et al.[41] The detailed procedures of the syntheses are given in the Supporting Information (SI).

### Azide functionalization of block copolymers

As the triblock copolymer, Synperonic F108 (poly(ethylene glycol)-*block*-poly(propylene glycol)-*block*-poly(ethylene glycol), purchased from Sigma-Aldrich) is employed. As the diblock copolymer, polystyrene-*block*-poly(ethylene glycol) is synthesized according to Caciagli et al.[31] Subsequently, both of the block copolymers are functionalized with azide using a tosylation reaction to make them suitable for Cu-free click-reaction to connect the single-stranded DNAs. Briefly, block copolymers are first tosylated using tosyl chloride and subsequently, the tosyl groups are exchanged with azide groups using $NaN_3$ as described in Reference 31.

### Supraparticle preparation

Prior to the preparation of the SPs, the NPs in nonpolar solvents are mixed with ethanol and precipitated using centrifuge. Subsequently, they are dispersed again in a nonpolar solvent immiscible with water (e.g., cyclohexane, hexane, or hexadecane) such that the final nanoparticle concentration in the dispersion becomes 5 mg/mL. In a separate flask, a solution of azide-functionalized block copolymers is prepared using ultrapure water at a concentration of 2% w/v. To better dissolve the polymer, the solution is kept at 4°C overnight, and filtered using a syringe filter with a pore size of 0.45 µm. Subsequently, 0.2 mL of the nanoparticle dispersion is added on to 1.8 mL of the polymer solution. The mixture is then vortexed for 15 min and ultrasonicated using a Bandelin Sonopulse HD 2200 probe sonicator at 20% amplitude for 10 min in pulsed mode at a frequency of 1 Hz with a sonication duty cycle of 50 percent. The caps of the vials containing the droplets of the NPs are left open at ambient temperature for at least 24 h so that the nonpolar solvent can evaporate.

### DBCO-functionalization of the single-stranded DNAs

NH-functionalized single-stranded DNAs were purchased from Integrated DNA Technologies (IDT). Two different strands that possess complementary chains are employed. These are α: NH-5′-TTT TTT TTT TTT TTT GGT GCT GCG-3′ and α′: NH-5′- TTT TTT TTT TTT TTT CGC AGC ACC-3′. To enable Cu-free click chemistry between the azide-functionalized block copolymers and the DNA molecules, NH groups of the DNA molecules are converted to dibenzocyclooctyne (DBCO) as described by Caciagli et al.[31] Briefly, DBCO-sulfo-NHS in dimethylsulfoxide (DMSO) (10 µL, 20 mM) was mixed with amine-functionalized DNAs (100 µL, 1 mM) in 10 mM phosphate buffered saline containing NaCl such that the final NaCl concentration is 100 mM. By keeping the mixture at 60°C on a shaker overnight, DBCO molecules replaced the amine groups on the DNA molecules and DBCO-functionalized DNA was obtained. The synthesized DBCO-DNA molecules were purified using Illustra NAP-25 columns. Obtained DBCO-functionalized DNA molecules were stored in a freezer at −20°C for subsequent use.

### DNA-functionalization of the SPs

Fifty µL of the azide-functionalized SPs dispersion was mixed with α or α′ DBCO-functionalized DNA (25 mmol, 500 µL) and the surfactant solution (i.e., not azide-functionalized diblock or triblock copolymer solution, 2% in phosphate buffer, 500 µL). The mixture was then shaken at 60°C. In order to increase the DNA loading, NaCl was added stepwise such that the final salt concentration becomes 100 mM in 2 h. The mixture was left to react for 24 h and the SPs were dialyzed against 0.5% surfactant solution in phosphate buffer using a 100 kDa dialyzer.

### Hybridization of the SPs

α- and α′-type DNA-functionalized SPs of equal volumes (100 μL) were mixed and a NaCl solution in phosphate buffer was added to the mixture such that the final NaCl concentration becomes 100 mM.

### Quantitative information on DNA-attachment of SPs

DNA-functionalized SPs (20 μL) were mixed with an excess amount of Cy5-functionalized complementary DNAs (5 μL, ~100 μM) in a solution of 0.1 M NaCl containing phosphate buffer. After an hour of hybridization, 100 μL of 1 M NaCl in phosphate buffer was added and the SPs were precipitated using centrifugation. The number of coated Cy5-functionalized DNAs was calculated by measuring the absorption of the Cy5 molecules in the supernatant. To obtain the information on the number of available azide molecules on the SPs, we added DBCO-functionalized Cy5 dyes (30 μL, 1 mM) on 25 μL of azide-functionalized SPs in a solution of 0.1 M of NaCl containing phosphate buffer. The mixture was kept at 60°C overnight followed by the precipitation of the SPs via centrifugation after adding an excess amount of salt as described above. The number of coated DBCO-Cy5 molecules was estimated by taking the absorption spectrum of the supernatant containing uncoated Cy5 molecules.

### Further characterizations

The Fourier transform infrared spectroscopy of the surfactants was carried out using a Spotlight 400 N FT-NIR system. The dynamic light-scattering and zeta-potential measurements were carried out using a Malvern Instruments ZetaSizer ZS90 system. Absorbance and fluorescence measurements were collected using a Cary UV–vis spectrophotometer and a Cary Eclipse fluorescence spectrophotometer, respectively. Scanning electron microscope and scanning transmission electron microscope images were taken using a Hitachi S-5500 SEM/STEM system.

## Results and discussion

We prepared these SPs by first creating a micellar system stabilized by amphiphilic surfactants. These micelles trapped the hydrophobic NPs (red-emitting InP/ZnSeS/ZnS core/shell/shell QDs, silver NPs, and iron oxide NPs) inside while the micelles themselves were dispersed in water. As illustrated in **Figure 1**, we formed these micelles by mixing the NPs in a hydrophobic solvent that is immiscible with water (such as chloroform, hexane, and cyclohexane) with an aqueous solution of amphiphilic azide-functionalized diblock ($N_3$-PEG-PS) or triblock ($N_3$-PEG-PPO-PEG-$N_3$) copolymers. Upon emulsification and treatment with a probe ultrasonicator, we obtained micelles containing NPs and hydrophobic solvent owing to the amphiphilic nature of the surfactant copolymers. Subsequently, we evaporated the solvent inside the micelles to create the SPs.

In our experiments, we assessed the use of various solvents that are immiscible with water to prepare our micelles. Since we were interested in the SPs in which there is no hydrophobic solvent remains, the use of solvents with high boiling points (e.g., toluene and hexadecane) would not be practical. On the other hand, a solvent with a low boiling point would easily evaporate during the ultrasonication leaving irregular chunks of NPs behind rather than micelles. To determine the suitable solvents, here we formed micelles of silver NPs, nanocrystal QDs, and iron oxide NPs using chloroform, hexane, and cyclohexane that have boiling temperatures of 61°C, 68°C, and 81°C, respectively. We observed that micelles prepared using chloroform and hexane were inhomogeneous and comprised of big chunks of nanoparticle-surfactant mixtures due to the quick evaporation of chloroform and hexane during sonication. Owing to the higher boiling point of cyclohexane, we were able to prepare nanoparticle-containing cyclohexane micelles that have a homogenous appearance. Similarly, we were able to prepare micelles with a homogenous appearance using solvents with even higher boiling points such as toluene and hexadecane. On the other hand, >100°C boiling points of these two latter solvents made it difficult to obtain the SPs as the duration of solvent evaporation is very long. Contrary to hexadecane and toluene, cyclohexane inside the micelles evaporated within a day when the cap of the vial was left open. Using dynamic light-scattering measurements, we confirmed that after one day the size of the SPs decreased to 52% of its size right after preparation and did not change after one day. As shown in Figure 1b, right after the cyclohexane micelles were prepared, the dispersion has a milky appearance because of the stronger scattering. Furthermore, different than the micelles prepared with hexane or chloroform, cyclohexane micelles do not include any chunks. As the solvent evaporates, the milky appearance of these micelles completely vanishes leading to translucent supraparticle dispersions. This variation in the scattering nature clearly indicates the reduction of the size and formation of a collection of particles free form solvents and stabilized by surfactant polymers.

The electron microscope images (**Figures 2** and S2), the hydrodynamic size measurements (**Figure 3**), and the polydispersity index calculations (Figure S3) reveal that the choice of the surfactant has a strong influence on the supraparticle size with a weak dependence on the type of NP dispersion used (silver NPs, QDs, and iron oxide NPs). According to electron microscope images, employing only diblock copolymers results in ~500-nm-sized SPs that possess irregular shapes (Figure 2a), whereas we observe ~50-nm-sized spherical SPs when we used diblock copolymers together with triblock copolymers or only triblock copolymers (Figure 2b and c, respectively). Although the hydrodynamic size measurements (Figure 3b–d) support our observations, we measured slightly larger sizes possibly not only due to the persistence length of the surfactants on SPs, but also owing to the effect of evacuation during the electron microscopy imaging. These results show that there is a clear difference in the stabilization of the SPs when different surfactants are employed. Employing

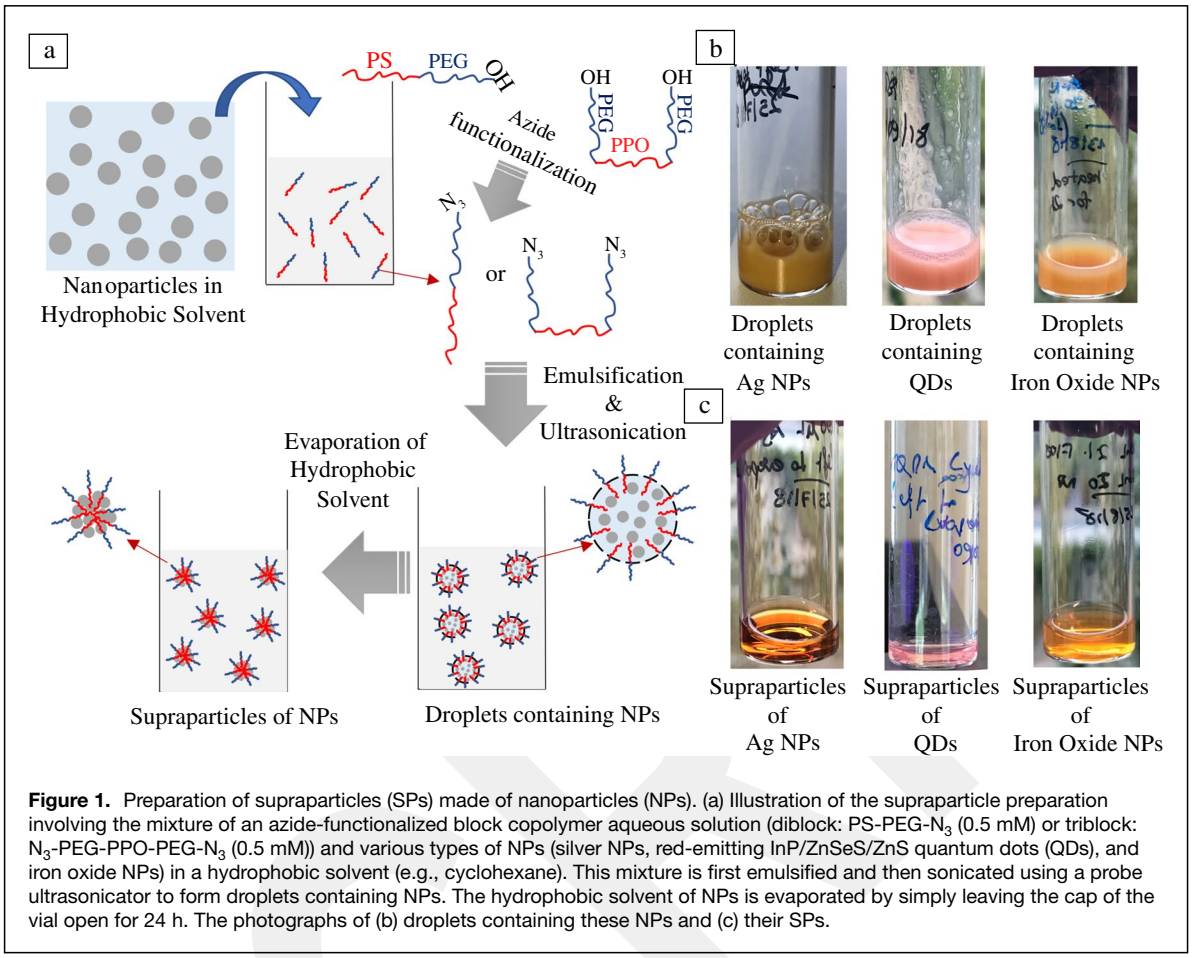


**Figure 1.** Preparation of supraparticles (SPs) made of nanoparticles (NPs). (a) Illustration of the supraparticle preparation involving the mixture of an azide-functionalized block copolymer aqueous solution (diblock: PS-PEG-$N_3$ (0.5 mM) or triblock: $N_3$-PEG-PPO-PEG-$N_3$ (0.5 mM)) and various types of NPs (silver NPs, red-emitting InP/ZnSeS/ZnS quantum dots (QDs), and iron oxide NPs) in a hydrophobic solvent (e.g., cyclohexane). This mixture is first emulsified and then sonicated using a probe ultrasonicator to form droplets containing NPs. The hydrophobic solvent of NPs is evaporated by simply leaving the cap of the vial open for 24 h. The photographs of (b) droplets containing these NPs and (c) their SPs.

diblock copolymers leads to larger sizes compared to the triblock copolymers, as also supported by Reference 42.

In order to self-assemble these SPs via DNA-DNA interaction, we next synthesized azide-functionalized block copolymers. In short, we converted the OH groups on the surfaces of the surfactant molecules to tosylates by reacting the polymers first with tosyl chloride. In the second step of the reaction, we converted the tosylate groups to azide groups ($N_3$) by reacting the polymers with $NaN_3$. We then employed these $N_3$-functionalized block copolymers in the preparation of the SPs of silver NPs, semiconductor QDs, and iron oxide NPs. After this step, we attached single-stranded alkyne-functionalized DNAs on the surfaces of the SPs through copper-free click chemistry. The zeta-potential measurements showed shifts toward negative values indicating the successful attachment of the DNA molecules on to the surfaces of the SPs. We observe that this shift is more prominent for all types of SPs when only diblock copolymers are employed. For the silver SPs, the shift becomes the smallest when only triblock copolymers are employed, whereas for iron oxide and QD SPs this shift is the smallest when diblock and triblock copolymers are employed together. Since the surfactant polymers are nonionic, these shifts are direct indicators of the DNA-attachment process. To obtain quantitative information on DNA-attachment, we added

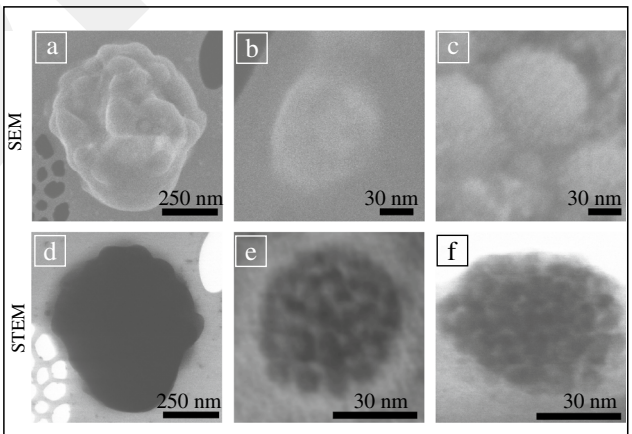


**Figure 2.** Electron microscope images of supraparticles (SPs) prepared using different block copolymers. Scanning electron microscope (SEM) images of SPs of quantum dots made using (a) diblock polymer (0.5 mM), (b) diblock and triblock polymer mixture (both 0.5 mM), and (c) triblock polymer (0.5 mM). Scanning transmission electron microscope (STEM) images of the SPs made using (d) diblock polymer, (e) diblock and triblock polymer mixture, and (f) triblock polymer.

Cy5 dye-functionalized complementary single-stranded DNA to the DNA-functionalized supraparticle dispersion. Based on

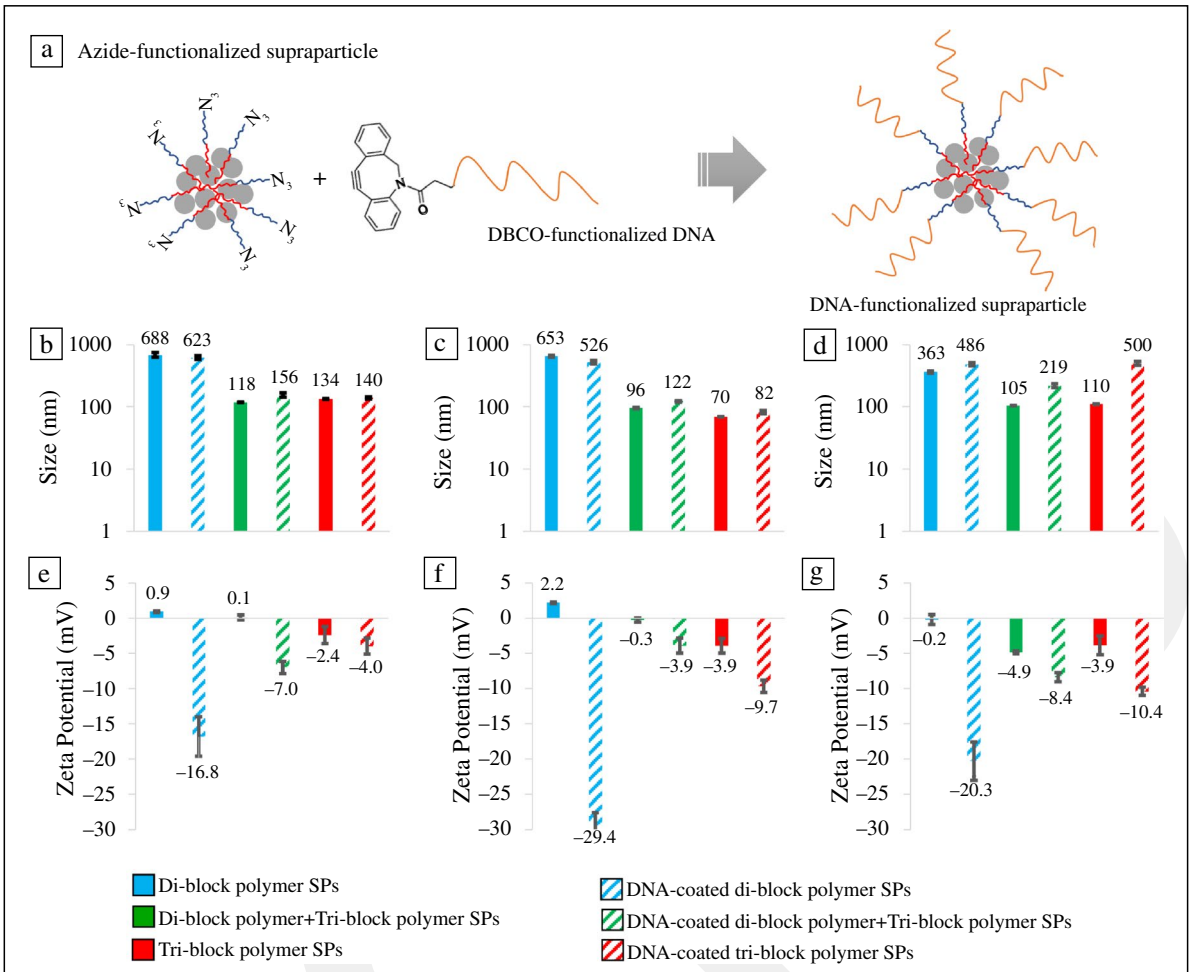


**Figure 3.** Size and zeta potential of supraparticles (SP)s with and without DNA-functionalization. (a) Illustration of the DNA coating process of the SPs through copper-free click chemistry involving azide groups of the surfactants and DBCO groups of the DNA. Size information obtained through dynamic light-scattering measurements of DNA-functionalized and non-DNA-functionalized SPs of (b) silver nanoparticles (NPs), (c) nanocrystal quantum dots (QDs), and (d) iron oxide NPs. Zeta potential of DNA-functionalized and non-DNA-functionalized SPs of (e) silver NPs, (f) nanocrystal QDs, and (g) iron oxide NPs. The numbers in the plots indicate the average of three measurements, whereas the error bars stand for the standard deviation of these measurements.

the absorption measurements of the dye-functionalized DNAs, we calculated the concentration of the DNAs that were successfully attached to the SPs as it was also presented in Reference 43. Results presented in Figure S5 indicate that for QDs and iron oxide NPs the hybrid use of diblock and triblock copolymers becomes the most successful approach, whereas for the silver SPs the optimal choice turns out to be the use of only diblock copolymers. This dependence may stem from the differences in the number of available azide molecules on the SP, but also from the different ligands of various types of NPs. To analyze the available azide groups on the SPs, we attached DBCO-functionalized Cy5 dyes through Cu-free click chemistry to the SPs. Since these dyes are much smaller molecules than the DNAs, we expect them to attach easier to the surface of the particles and aim to get information on the number of available azide groups on the surfaces of the SPs. Our results presented in Figure S4 show that silver and QD SPs stabilized with diblock copolymers have a significantly higher number of available azide molecules. For iron oxide SPs, however, the highest number of available azide molecules appeared when triblock and diblock copolymers are used together. These results reveal that for silver and iron oxide SPs, DNA-attachment efficiency correlates very well with the available number of azide groups on the surface. For QD SPs, however, DNA-attachment is more efficient when diblock and triblock copolymers are employed together despite that the SPs prepared using only diblock copolymers have more available azide groups. We believe that this may be caused by the free ligands of the NPs that may end up on the surface of the SPs; however, further investigation is necessary on this matter. Based on the data presented in Figures S4 and S5, we estimated the number of dye molecules and

DNAs per supraparticle using the methodology described in the ESM. The results presented in Tables S1 and S2 indicate that the numbers of available azide groups and the DNAs per supraparticle are significantly higher for the SPs made of only diblock copolymer due to their large sizes. When only triblock copolymer or diblock and triblock copolymer mixtures are used as the surfactant, for all the nanoparticle types the number of available azide groups per supraparticle becomes similar within the range of an order of magnitude. Nevertheless, it is worth noting that the QD SPs possess the lowest number of available azide groups per SP, which may be due to the interaction of the surfactant with the ligands of the QDs. As a result, the number of DNA molecules connected to the SPs prepared with triblock and the hybrid of triblock and diblock copolymers remains lowest for the QD supraparticles.

When we compare the absorbance characteristics of the SPs (**Figure 4**), we observe that silver SPs and QD SPs have very similar absorption spectra with and without DNA- attachment for triblock copolymers along with diblock and triblock copolymers. This indicates that the ligands of the NPs keep the NPs inside the supraparticle separated enough such that the absorption spectra do not vary significantly. On the other hand, the large sizes of the SPs of all NPs prepared using diblock copolymers reveal itself with an increase in the absorbance levels with and without DNA-functionalization due to scattering, which does not allow for any comparison with the nanoparticles and SPs with other surfactants.

In the next step of our experiments, we wanted to utilize the DNA-driven self-assembly and magnetic features of the iron oxide NP containing SPs to alter the optical properties of the material system. For this purpose, we hybridized QD SPs and iron oxide NP SPs that are functionalized with complementary single-stranded DNAs. The network formation was confirmed with the shift in the melting temperature measurements from 32°C for the DNAs unconnected to the SPs to beyond 40°C for the SPs possessing complementary DNAs (Figure S6).

We further applied magnetic field to the network formed by iron oxide and QD SPs and demonstrated a control mechanism on the optical polarization of the light emitted by the QDs. A neodymium magnet enabled the magnetization of the iron oxide SPs causing structural changes in the DNA-functionalized SP network made of QDs and iron oxide NPs. Since the applied magnetic field in the vertical direction would lead to the alignment of the iron oxide SPs (**Figure 5**a), we expected to achieve a polarization-selective light transmission similar to the effect caused by magnetically aligned metal nanowire and QD hybrids as observed by Uran et al.[44] Our results presented in Figure 5b show that in the absence of the magnetic field, the PL intensity of the hybridized DNA-functionalized QD and iron oxide NP SPs decreased compared to the case of only DNA-functionalized QD-SPs. Furthermore, the hybridization of these SPs did not result in any polarization dependence of the QD emission when no magnetic field was applied. On the other hand, upon application of the magnetic field, we observed anisotropy in the emission polarization of the QD-SPs in the hybrid system when we employed SPs prepared using triblock and diblock copolymers together. In these samples, the intensity of the QD emission decreased by ca. 30% compared to the emission intensity of only DNA-functionalized QD-SPs at 0° polarization angle, whereas the emission intensity increased by ~20% at 90° polarization angle resulting in a polarization ratio of 1.9.

Another interesting observation is that at around 90° polarization angle the PL intensity of the hybrid supraparticle network takes its maximum value that is even higher than the intensity of the only QD SPs. This may be caused by the fact that the QD-SPs that form a network with the iron oxide NP-SPs get closer to each other compared to the case of isolated QD-SPs in solution. As a result, the light source may excite more QDs when the hybrid SPs are employed, whereas the number of QDs excited may remain lower when the SPs are isolated.

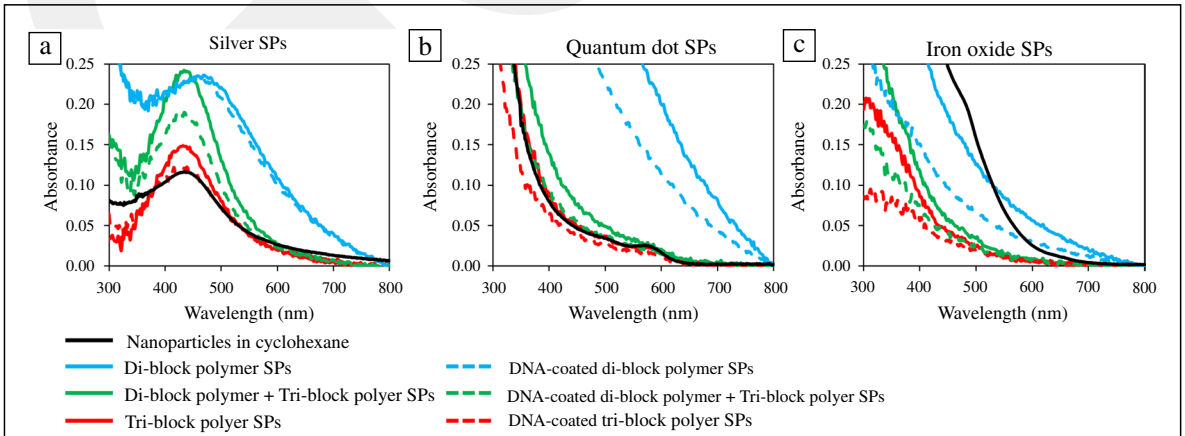


**Figure 4.** Absorption spectra of supraparticles (SPs) prepared using (a) silver nanoparticles (NPs), (b) quantum dots, and (c) iron oxide NPs.

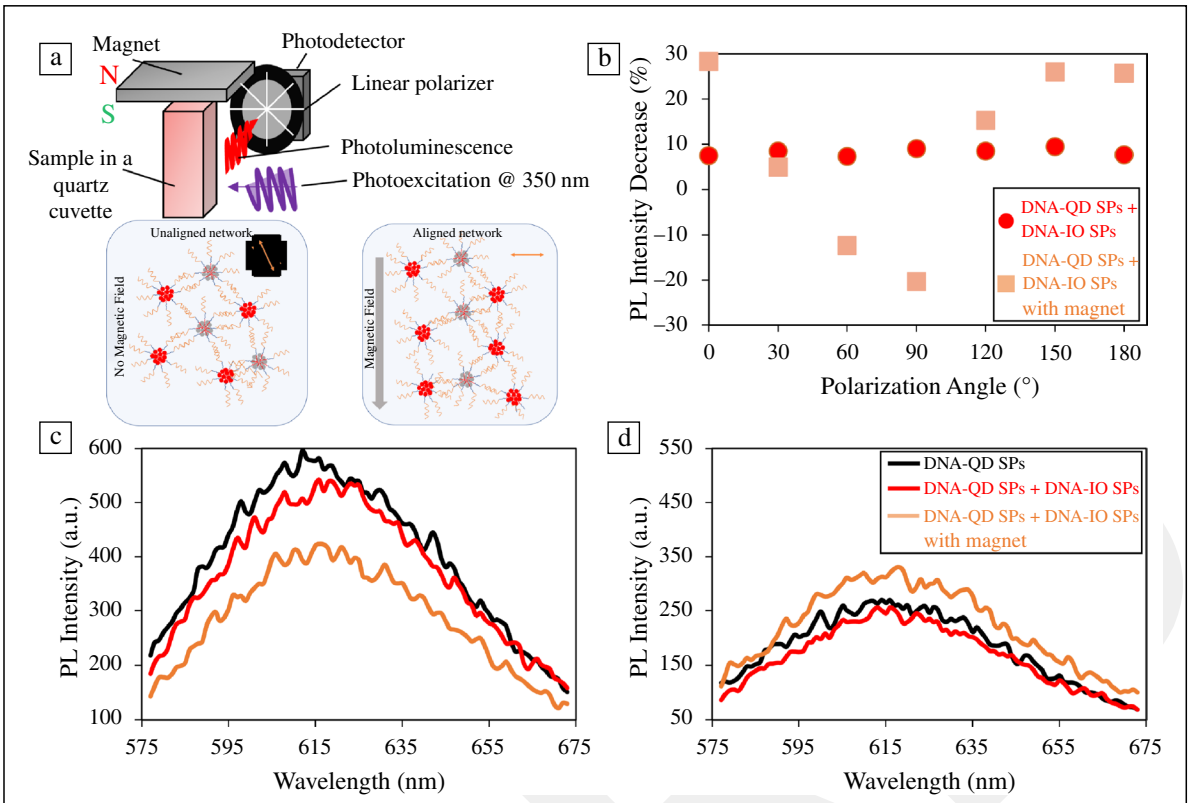


**Figure 5.** Emission polarization of emitted light from a DNA-functionalized quantum dot (QD) supraparticle (SP) and DNA-functionalized iron oxide (IO) nanoparticle (NP) SP network upon application of magnetic field. (a) Illustration of the experimental setup and restructuring of the network in response to the magnetic field. Samples (DNA-functionalized QD SPs alone, and the hybrid made of QD and IO NP SPs having complementary DNAs) are loaded into a quartz cuvette and photoluminescence (PL) measurements at different polarizations are recorded at different polarization angles. (b) Decrease in the integrated PL intensity of the samples prepared using diblock and triblock polymers, with and without the application of magnetic field at different polarizations. The intensity decrease is calculated by using the emission intensity of only DNA-functionalized QD SPs at the same polarizations. (c) PL spectra of these samples with and without the application of magnetic field at 0° polarization. (d) PL spectra of these samples with and without the application of magnetic field at 90° polarization.

The strength of the polarization dependence of the emission was also affected by the type of surfactant used (Figure S7). When we employed the SPs prepared using only triblock copolymers, there was no significant polarization dependence of the emission intensity under magnetic field. A polarization ratio of only 1.2 could be recorded in the case that the SPs prepared using only diblock polymers were employed. We think that the number of DNAs that could be attached to the SPs plays a key role here. When the number is low, the number of DNAs connecting the SPs is lower causing the formation of a weaker network. As a result, the magnetic field hardly reshapes the network leading to a much less pronounced polarization response.

## Conclusion

In this article, we report the DNA-functionalized SPs stabilized with amphiphilic block copolymers that form a network whose optical properties can be controlled by an externally applied magnetic field. These SPs are stabilized with azide-functionalized diblock and triblock copolymers, and consist of magnetic iron oxide NPs, plasmonic silver NPs, and semiconducting InP/ZnSeS/ZnS core/shell/shell QDs. We observed that the size of these SPs relies strongly on the type of the copolymer while no dependence was recorded on the type or ligand of the NPs, with diblock copolymers producing larger particles (~500 nm) than the triblock copolymers or a combination of diblock and triblock copolymers (~100 nm). Employing the azide-alkyne chemistry, we then coated these SPs with single-stranded DNA molecules and formed networks by hybridizing SPs having complementary DNA chains. After hybridizing QD and iron oxide SPs at room temperature, we studied the polarization of the QDs inside the network of SPs formed with iron oxide NPs. Applying a magnetic field reshaped the supraparticle network aligning iron oxide SPs and led to anisotropic emission with a polarization ratio of ~2 from the QDs-containing-SPs that emit isotropic light in the absence of the magnetic field.

This article shows that the DNA-driven self-assembly of nanostructures can be utilized to control the optical

properties of the material systems using external excitations. The applicability to utilize new control mechanisms will further broaden the use of this smart self-assembly technique in optics and photonics.

## Acknowledgments

T.E. acknowledges The Royal Society for the Newton International Fellowship.

## Funding

T.E. acknowledges The Royal Society for the Newton International Fellowship. M.Z. would like to acknowledge EPSRC and Unilever for the CASE Award RG748000. A.C. and E.E. acknowledge the ETN-COLLDENSE (H2020-MCSA-ITN-2014, Grant No. 642774). E.E. acknowledges the support of the Research Council of Norway through its Centres of Excellence funding scheme, Project No. 262644. T.O'N. thanks the Nano-Doctoral Training Centre, funded through the EPSRC.

## Data availability

The data sets generated during and/or analyzed during the current study are available from the corresponding author on reasonable request.

## Conflict of interest

On behalf of all the authors, the corresponding authors state that there is no conflict of interest.

## Supplementary Information

The online version contains supplementary material available at https://doi.org/10.1557/s43577-022-00352-z.

## References

1. H.J. Yun, J. Lim, J. Roh, D.C.J. Neo, M. Law, V.I. Klimov, *Nat. Commun.* **11**, 5280 (2020)
2. L. Chouhan, S. Ghimire, C. Subrahmanyam, T. Miyasaka, V. Biju, *Chem. Soc. Rev.* **49**(10), 2869 (2020)
3. T. Erdem, H.V. Demir, *Nanophotonics* **5**(1), 74 (2016). https://doi.org/10.1515/nanoph-2016-0009
4. K. Roh, C. Dang, J. Lee, S. Chen, J.S. Steckel, S. Coe-Sullivan, A. Nurmikko, *Opt. Express* **22**(15), 18800 (2014). https://doi.org/10.1364/OE.22.018800
5. B. Liu, Y. Altintas, L. Wang, S. Shendre, M. Sharma, H. Sun, E. Mutlugun, H.V. Demir, *Adv. Mater.* **32**(8), 1905824 (2020). https://doi.org/10.1002/adma.201905824
6. A. Bajpai, S. Carlotti, *Nanomaterials* **9**(7), 1057 (2019). https://doi.org/10.3390/nano9071057
7. P. Xu, T. Erdem, E. Eiser, *Soft Matter* **16**(23), 5497 (2020). https://doi.org/10.1039/c9sm01585j
8. W. Poon, B.R. Kingston, B. Ouyang, W. Ngo, W.C.W. Chan, *Nat. Nanotechnol.* **15**, 819 (2020). https://doi.org/10.1038/s41565-020-0759-5
9. K. Yu, T. Fan, S. Lou, D. Zhang, *Prog. Mater. Sci.* **58**(6), 825 (2013). https://doi.org/10.1016/j.pmatsci.2013.03.003
10. T.-H. Kim, K.-S. Cho, E.K. Lee, S.J. Lee, J. Chae, J.W. Kim, D.H. Kim, J.-Y. Kwon, G. Amaratunga, S.Y. Lee, B.L. Choi, Y. Kuk, J.M. Kim, K. Kim, *Nat. Photonics* **5**, 176 (2011). https://doi.org/10.1038/NPHOTON.2011.12
11. E. Fisslthaler, S. Sax, U. Scherf, G. Mauthner, E. Moderegger, K. Landfester, E.J.W. List, *Appl. Phys. Lett.* (2008). https://doi.org/10.1063/1.2921780
12. Y. Altintas, I. Torun, A.F. Yazici, E. Beskazak, T. Erdem, M. Serdar Onses, E. Mutlugun, *Chem. Eng. J.* (2020). https://doi.org/10.1016/j.cej.2019.122493
13. R.J. Macfarlane, B. Lee, M.R. Jones, N. Harris, G.C. Schatz, C.A. Mirkin, *Science* 80 **334**(6053), 204 (2011). https://doi.org/10.1126/science.1210493
14. N. Liu, T. Liedl, *Chem. Rev.* **118**(6), 3032 (2018). https://doi.org/10.1021/acs.chemrev.7b00225
15. O. Erdem, S. Foroutan, N. Gheshlaghi, B. Guzelturk, Y. Altintas, H.V. Demir, *Nano Lett.* **20**(9), 6459 (2020). https://doi.org/10.1021/acs.nanolett.0c02153
16. S. Foroutan-Barenji, O. Erdem, N. Gheshlaghi, Y. Altintas, H.V. Demir, *Small* **16**(45), 2004304 (2020). https://doi.org/10.1002/smll.202004304
17. Y. Chen, Y. Fu, X. Li, H. Chen, Z. Wang, H. Zhang, *RSC Adv.* **9**(30), 17093 (2019). https://doi.org/10.1039/c9ra02135c
18. C.R. Forest, C.A.C. Silva, P. Thordarson, *Pept. Sci.* (Hoboken) (2021). https://doi.org/10.1002/pep2.24205
19. H.V. Demir, U.O.S. Seker, G. Zengin, E. Mutlugun, E. Sari, C. Tamerler, M. Sarikaya, *ACS Nano* **5**(4), 2735 (2011). https://doi.org/10.1021/nn103127v
20. R. Ma, R. Kong, Y. Xia, X. Li, X. Wen, Y. Pan, X. Dong, *Appl. Phys. Lett.* **113**(3), 033702 (2018). https://doi.org/10.1063/1.5037522
21. D.B. Litt, M.R. Jones, M. Hentschel, Y. Wang, S. Yang, H.D. Ha, X. Zhang, A.P. Alivisatos, *Nano Lett.* **18**(2), 859 (2018). https://doi.org/10.1021/acs.nanolett.7b04116
22. L. Di Michele, F. Varrato, J. Kotar, S.H. Nathan, G. Foffi, E. Eiser, *Nat. Commun.* **2013**, 4 (2007). https://doi.org/10.1038/ncomms3007
23. Y. Tian, Y. Zhang, T. Wang, H.L. Xin, H. Li, O. Gang, *Nat. Mater.* **15**(6), 654 (2016). https://doi.org/10.1038/nmat4571
24. C.A. Mirkin, R.L. Letsinger, R.C. Mucic, J.J. Storhoff, *Nature* **382**(6592), 607 (1996). https://doi.org/10.1038/382607a0
25. A.P. Alivisatos, K.P. Johnsson, X. Peng, T.E. Wilson, C.J. Loweth, M.P. Bruchez, P.G. Schultz, *Nature* **382**(6592), 609 (1996). https://doi.org/10.1038/382609a0
26. L. Sun, H. Lin, K.L. Kohlstedt, G.C. Schatz, C.A. Mirkin, *Proc. Natl. Acad. Sci. U.S.A.* **115**(28), 7242 (2018). https://doi.org/10.1073/pnas.1800106115
27. D. Sun, O. Gang, *J. Am. Chem. Soc.* **133**(14), 5252 (2011). https://doi.org/10.1021/ja111542t
28. S.Y. Park, A.K.R. Lytton-Jean, B. Lee, S. Weigand, G.C. Schatz, C.A. Mirkin, *Nature* **451**(7178), 553 (2008). https://doi.org/10.1038/nature06508
29. C.R. Laramy, M.N. O'Brien, C.A. Mirkin, *Nat. Rev. Mater.* **4**(3), 201 (2019). https://doi.org/10.1038/s41578-019-0087-2
30. M. Zupkauskas, Y. Lan, D. Joshi, Z. Ruff, E. Eiser, *Chem. Sci.* **8**(8), 5559 (2017). https://doi.org/10.1039/C7SC00901A
31. A. Caciagli, M. Zupkauskas, A. Levin, T.P.J. Knowles, C. Mugemana, N. Bruns, T. O'Neill, W.J. Frith, E. Eiser, *Langmuir* **34**(34), 10073 (2018). https://doi.org/10.1021/acs.langmuir.8b01828
32. S. Wintzheimer, T. Granath, M. Oppmann, T. Kister, T. Thai, T. Kraus, N. Vogel, K. Mandel, *ACS Nano* **12**(6), 5093 (2018). https://doi.org/10.1021/acsnano.8b00873
33. J. Lacava, A.A. Ouali, B. Raillard, T. Kraus, *Soft Matter* **10**(11), 1696 (2014). https://doi.org/10.1039/c3sm52949e
34. F. Montanarella, D. Urbonas, L. Chadwick, P.G. Moerman, P.J. Baesjou, R.F. Mahrt, A. Van Blaaderen, T. Stöferle, D. Vanmaekelbergh, *ACS Nano* **12**(12), 12788 (2018). https://doi.org/10.1021/acsnano.8b07896
35. F. Montanarella, T. Altantzis, D. Zanaga, F.T. Rabouw, S. Bals, P. Baesjou, D. Vanmaekelbergh, A. Van Blaaderen, *ACS Nano* **11**(9), 9136 (2017). https://doi.org/10.1021/acsnano.7b03975
36. S. Paterson, S.A. Thompson, J. Gracie, A.W. Wark, R. De La Rica, *Chem. Sci.* **7**(9), 6232 (2016). https://doi.org/10.1039/c6sc02465c
37. M. Ma, H. Zhu, J. Ling, S. Gong, Y. Zhang, Y. Xia, Z. Tang, *ACS Nano* **14**(4), 4036 (2020). https://doi.org/10.1021/acsnano.9b08570
38. J. Guo, W. Yang, C. Wang, *Adv. Mater.* **25**(37), 5196 (2013). https://doi.org/10.1002/adma.201301896
39. J.-H. Jo, J.-H. Kim, K.-H. Lee, C.-Y. Han, E.-P. Jang, Y.R. Do, H. Yang, *Opt. Lett.* **41**(17), 3984 (2016). https://doi.org/10.1364/ol.41.003984
40. Y. Altintas, M.Y. Talpur, M. Ünlü, E. Mutlugün, *J. Phys. Chem. C* **120**(14), 7885 (2016). https://doi.org/10.1021/acs.jpcc.6b01977
41. Z. Farrell, C. Shelton, C. Dunn, D. Green, *Langmuir* **29**(30), 9291 (2013). https://doi.org/10.1021/la305133d
42. Y.W. Yang, N.J. Deng, G.E. Yu, Z.K. Zhou, D. Attwood, C. Booth, *Langmuir* **11**(12), 4703 (1995). https://doi.org/10.1021/la00012a021
43. C. Zhang, R.J. Macfarlane, K.L. Young, C.H.J. Choi, L. Hao, E. Auyeung, G. Liu, X. Zhou, C.A. Mirkin, *Nat. Mater.* **12**(8), 741 (2013). https://doi.org/10.1038/nmat3647
44. C. Uran, T. Erdem, B. Guzelturk, N.K. Perkgöz, S. Jun, E. Jang, H.V. Demir, *Appl. Phys. Lett.* **105**(14), 141116 (2014). https://doi.org/10.1063/1.4897971